

Ultra-Wideband Antenna-Induced Error Prediction using Deep Learning on Channel Response Data

Janis Tiemann, Johannes Pillmann and Christian Wietfeld
TU Dortmund University, Communication Networks Institute (CNI)
Otto-Hahn-Str. 6, 44227 Dortmund, Germany
{janis.tiemann, johannes.pillmann, christian.wietfeld}@tu-dortmund.de

Abstract—Ultra-wideband wireless positioning technologies based on IEEE 802.15.4a have gained attention for various use cases requiring highly precise localization. In this paper the orientation dependent characteristics of commonly used ultra-wideband modules are experimentally determined and analyzed. The specific challenge addressed in this paper is the prediction of orientation induced ranging errors through channel response analysis. For the in-depth validation of the proposed methodology, two experiments are performed: the first one is conducted indoors to demonstrate the system behavior in dense multipath environments, whereas the second experiment is executed in an outdoor environment to allow for detailed analysis with as few multipath components as possible. In a second step, a deep learning neural network is applied to the channel response data, showing that the orientation induced ranging error estimate can be improved significantly using the proposed method.

Keywords—Ultra-wideband (UWB), Wireless Positioning, Channel Response Analysis, Deep Learning, Error Prediction, Antenna Characteristics.

I. INTRODUCTION AND RELATED WORK

Recent developments in Ultra-Wideband (UWB) hardware enabled low-cost time of arrival (TOA) based wireless localization. The reason UWB is a viable candidate for reliable and accurate positioning is the use of very short pulses that correspond to the large bandwidth. In the UWB physical layer (PHY) of IEEE 802.15.4a bandwidths from 500 MHz to 1 GHz are defined [1]. The signal is modulated using Burst-Position Modulation Binary Phase-Shift Keying (BPM-BPSK) using pulses with a pulse duration of either 2 ns or 0.92 ns. Through those rather short pulses the receiver is enabled to differentiate between the direct path and most indirect paths through cross-correlation of the received signal with the reference pulse.

Previous research investigated the use of UWB transceivers for indoor unmanned aerial vehicle (UAV) navigation [2] and for precision parking in electric vehicle (EV) charging scenarios [3]. It was shown that in the laboratory environment the accuracy of UWB is sufficient for precision alignment in the sub 10cm range. However, the results also showed a reproducible error pattern which can be shown using the raw data provided alongside [3]. Due to the reproducibility, the error pattern is suspected to be mainly caused by antenna characteristics and the influence of close indirect paths to the leading edge detection algorithm of the transceiver manufacturer.

This work aims to experimentally investigate the dependency of antenna orientation on the ranging results and the corresponding parameters and proposes the use of channel

response analysis to predict the ranging error and improve accuracy and reliability of UWB based ranging. Therefore, two experiments using controlled rotation around each axis in three-dimensional space will be conducted. The first is an indoor experiment, whereas the second experiment is conducted outdoors.

Similar experiments have been performed by [4]. However, only the absolute error was investigated using a body-mounted antenna. Dense in-vehicle multipath experiments were conducted in [5] for the 3 GHz to 11 GHz band and the 55 GHz to 65 GHz band. The channel impulse response for different orientations was analyzed. However, only four different orientations were chosen. Rudimentary qualification of ranging results are proposed by the manufacturer of the used UWB modules [6]. The method is based on the power of the first three components of the channel response compared to the energy of the full response and will be detailed in section II.

A more detailed analysis is given in [7]. The authors analyze the channel impulse response and the the vendor specific leading edge detection (LDE) in different scenarios. A method to differentiate erroneous range measurements is proposed and evaluated for the given scenarios. In [8] the exploitation of multipath for precise localization is proposed. Several approaches including simultaneous localization and mapping using multipath channel information or passive localization are considered.

In contrast to [7] and [8], this work proposes the consideration of the directional characteristics of the chosen module to eliminate errors introduced by the antenna orientation through deep learning. In the next sections an extensive experimental analysis of the orientational characteristics of the used modules is provided. The feasibility of the proposed method is evaluated experimentally.

II. RANGING CLASSIFICATION

In order to qualitatively classify ranging results, decaWave, the manufacturer of the DW1000 modules used in this work, proposes a first path analysis method [6]. The module provides registers with diagnostic information such as listed in Tab. I.

To assess the properties of the received packets, the diagnostics information is used. The manufacturer provided a way to reconstruct an estimation of the power of the first path P_{fp} from the recorded channel impulse response (CIR) registers as denoted in (1).

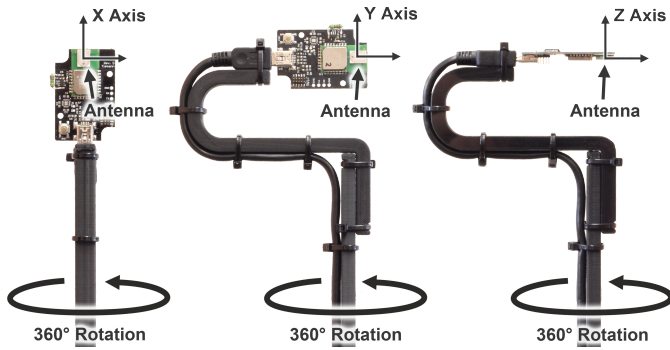


Fig. 1. Illustration of the axes of rotation chosen in the following experiments. The module is mounted on different 3D-printed holders to ensure rotation around each axis with minimal interference through the mounts.

$$P_{fp} = 10 \log_{10} \left(\frac{F_1^2 + F_2^2 + F_3^2}{N_p^2} \right) - A \text{ [dBm]} \quad (1)$$

The estimation of the accumulated power of the CIR P_{cir} is calculated as given in (2). This is representing the sum of the energy of all paths arriving, where A is a constant depending on the pulse repetition frequency (PRF) of the channel configuration used for communication. For instance, for a PRF set to 15.6 MHz $A=115.72$, for 62.4 MHz $A=121.74$.

$$P_{cir} = 10 \log_{10} \left(\frac{C \times 2^{17}}{N_p} \right) - A \text{ [dBm]} \quad (2)$$

A new metric, the first path ratio ϕ_{fp} is used to distinguish between line-of-sight (LOS) and non-line-of-sight (NLOS). The first path ratio is calculated as the difference of P_{fp} and P_{cir} , see (3). Since P_{fp} and P_{cir} are calculated as logarithmic values, the difference in logarithmic scale shows the ratio of both powers.

$$\phi_{fp} = P_{fp} - P_{cir} \quad (3)$$

A reflected signal holds less power and is more ambiguous than a signal received from the direct path, due to multiple interfering reflections, hence the first path ratio gives an indicator for possible NLOS conditions. A rule of thumb provided by decaWave defines the case-decision for NLOS detection of the received signal RX , see (4).

$$RX = \begin{cases} LOS & \text{for } \phi_{fp} > -6dB \\ LOS/NLOS & \text{for } -6dB > \phi_{fp} > -10dB \\ NLOS & \text{for } -10dB > \phi_{fp} \end{cases} \quad (4)$$

TABLE I. ULTRA-WIDEBAND MODULE DIAGNOSTIC REGISTERS.

type	name	description
uint16_t	F_1	LDE algorithm's first path amplitude at the first tap
uint16_t	F_2	LDE algorithm's first path amplitude at the second tap
uint16_t	F_3	LDE algorithm's first path amplitude at the third tap
uint16_t	C	Sum of the squares of magnitude of the accumulator
uint16_t	N_p	Preamble accumulator count
uint16_t	STD_NOISE	Standard deviation of the LDE noise level

Ranges with a ϕ_{fp} over -6 dB are detected as LOS, ranges with ϕ_{fp} under -10 dB are detected as NLOS. Between -6 dB and -10 dB there is an ambiguous zone of ϕ_{fp} where a clean distinction between LOS/NLOS is environment-specific, due to the unpredictable properties of the multipath propagation. However, the first path ratio is not suited to be used for error prediction, but rather as an outlier detection mechanism.

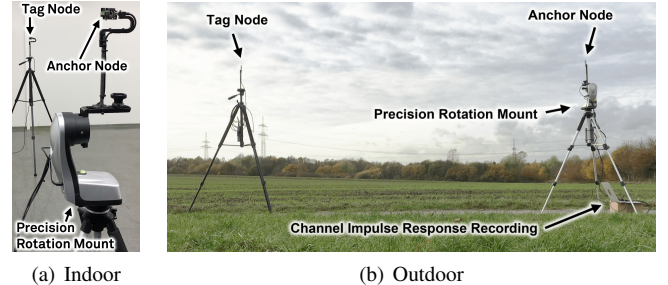


Fig. 2. Experimental setup of the outdoor experiment. The tag is static, the anchor is rotated with a precisely controllable rotation mount. The distance between tag and anchor is 3.57 m. Note that the experiment depicted indoors is the rotation around the Y axis at the starting position. The rotation angle is $\theta = 0$ for the depicted experiments.

III. EXPERIMENTAL EVALUATION

In order to quantify the directional properties of the UWB node, two experiments were conducted. An outdoor experiment is performed to determine the system characteristics with the presence of as few paths as possible. An indoor experiment is used to quantify the modules capabilities in the presence of multiple indirect paths.

The experimental setup of the outdoor experiment is depicted in Fig. 2. The tag node is statically mounted on a tripod. The anchor node is mounted on a precision rotation mount, that is controlled by the same unit that records the channel response data. The mount is rotated exactly 1° around the axis orthogonal to the ground surface with an interval of ten measurements. The rotation starts with θ at 0° and the antennas of the modules are facing each other symmetrically. The tag and the anchor continuously conduct symmetric double-sided two-way ranging (SDS-TWR). The channel response from the final message received at the anchor is recorded and used in the following evaluations. The channel configuration listed in Tab. II is used for the UWB PHY. Where f_c is the center frequency, B the used bandwidth, n_{prc} the number of bursts per chip, f_{pr} the mean pulse repetition frequency frequency, R the resulting average datarate, c_{pr} the spreading code number and n_{pr} the number of preamble symbols.

Both, the indoor and the outdoor experiments are conducted with the exact same parameters. To ensure comparability of the experimental results the raw datasets used for evaluation are provided alongside this work [9].

TABLE II. CHANNEL CONFIGURATION USED IN THE EXPERIMENTS.

f_c [GHz]	B [MHz]	n_{prc}	f_{pr} [MHz]	R [kbps]	c_{pr}	n_{pr}
6.4896	499.2	127	62.4	850	9	256

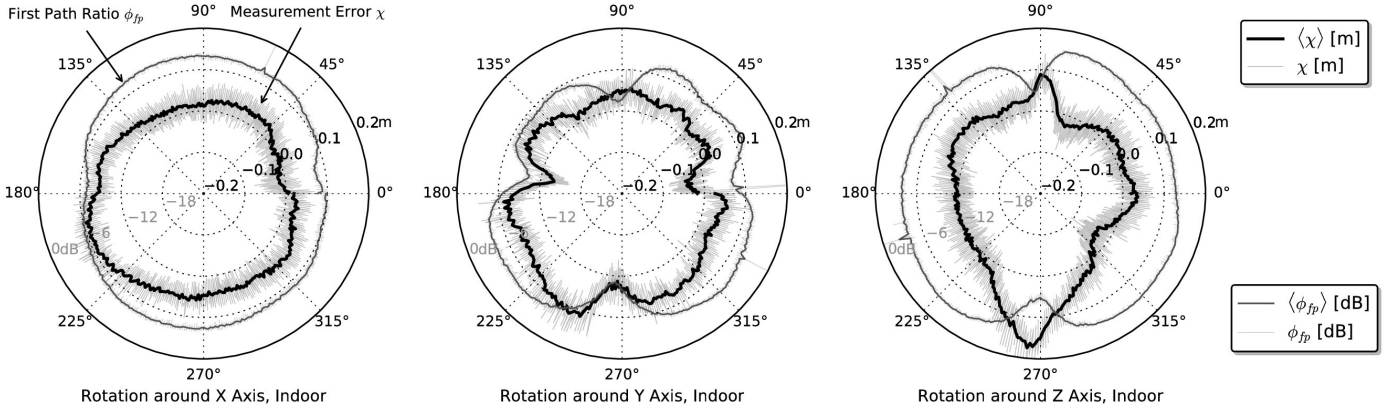


Fig. 3. Polarplot of the experimentally obtained raw and moving window filtered distance measurement error χ and $\langle\chi\rangle$ depending on the orientation angle θ in the indoor scenario. The first path ratio ϕ_{fp} and $\langle\phi_{fp}\rangle$ serves as an indicator for reduced receiving quality or non-line-of-sight (NLOS).

A. Orientation Dependent Ranging Error

Fig. 3 shows the experimentally measured ranging error χ and the average error over each degree $\langle\chi\rangle$ depending on the orientation angle θ in the indoor scenario. The rotation around the X axis is depicted on the lefthand side. A variation of up to 10 cm can be observed, depending on the rotation angle θ . However, the characteristics of the ranging error χ are comparably stable. The variation of the first path ratio ϕ_{fp} and the average first path ratio over each degree $\langle\phi_{fp}\rangle$ supports the notion, that the characteristics are stable around the X axis. Only flat and minor dents can be observed around 0° and 180° . The results of the rotation around the Y axis however, show major dents in the ranging error χ at 0° , 180° and 270° . Matching dents can be observed in the first path ratio ϕ_{fp} at 0° , 90° , 180° and 270° . The experimental results with rotation around the Z axis show a different pattern. The ranging error has bulges at 90° and 270° and corresponding dents in the first path ratio. Except for the dents, the first path ratio has a very regular pattern compared to the rotation around the Y axis.

Based on those results a suggestion for the mode of operation of the integrated modules is derived for minimal orientation induced errors. We suggest using the modules with the X axis upwards as this induces the least errors through change of orientation.

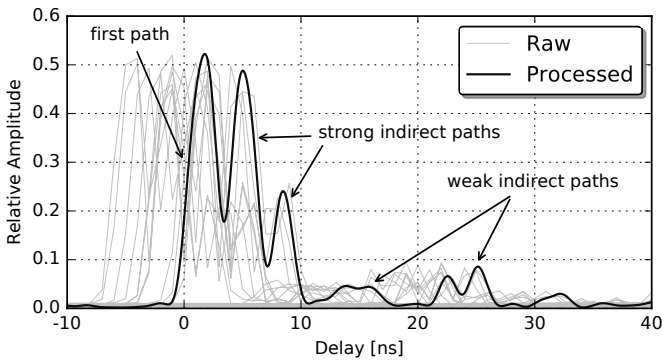


Fig. 4. Exemplary analysis of a single processed channel response. The raw data is aligned, interpolated and merged for future processable high resolution channel response analysis.

B. Channel Response Processing

Next to the ranging results, the raw accumulator data of the correlation registers are recorded in the above-mentioned experiments. This allows for orientation dependent channel response analysis. We propose deep learning to evaluate the capability of error prediction through pattern recognition.

In order to produce data for the deep learning algorithm, the raw accumulator data has to be processed as depicted in Fig. 4. In a first step the amplitude of the reference signal is determined calculating length of the quadrature component Q and the in-phase component I data of the accumulator registers. The channel response is not aligned in the registers. To align the data for further processing, the raw data is interpolated with a rate of $r = 10$ using biqubic interpolation. In a next step the indices are shifted using the first path index determined by the leading edge detection algorithm in the receiver. A final step averages all $n = 10$ interpolated channel response vectors for each rotation step.

C. Results of the Indoor Experiment

Fig. 5 depicts the processed channel response over the rotation angle θ . The heatmap represents the normalized relative amplitude of the processed channel response signals. The results are from the same experiment as shown in Fig. 3. The first experiment, rotating around the X axis shows strong direct paths at 90° and 270° . The remaining responses are distributed homogeneously with few variation of the indirect paths. A stronger indirect path is visible at around 10 ns, corresponding with the distance of nearby metal structures in the lab setup. The analysis of the rotation around the Y axis shows a much more scattered picture of the indirect paths received from the transceiver. The first path has strong dents at 0° , 90° , 180° and 270° . This corresponds directly with the results observed in Fig. 3. The rotation around the Z axis shows different results. Major dents in the first path are only visible at 90° and 270° . Those dents directly correspond with stronger indirect paths received starting at 20 ns delay. This is expected as the reception of signals through the electronics of the module is not possible. However, the reception capabilities of the module is also strongly limited facing the X axis.

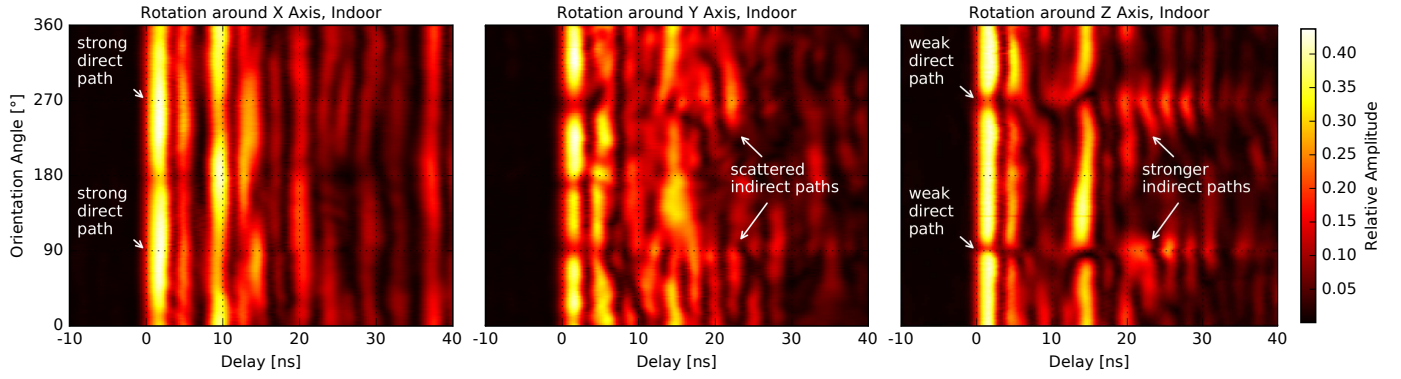


Fig. 5. Heatmap of the normalized relative amplitude of the orientation-dependent channel response in the indoor experiment. The channel response is recorded over the variation of the rotation angle θ . Note the different patterns of the channel response resulting from rotation around the different axes.

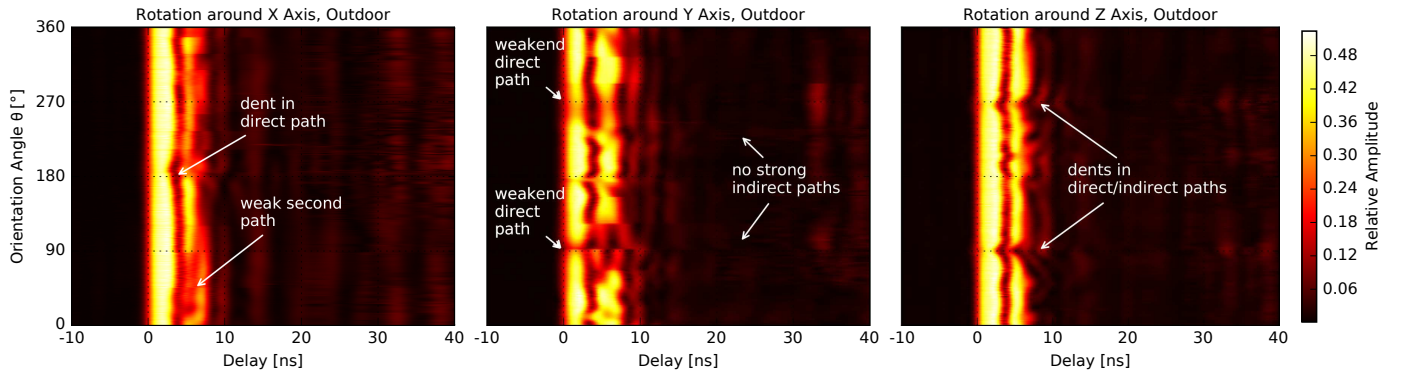


Fig. 6. Results from the outdoor experiment. Depicted is a heatmap of the normalized relative amplitude of the channel response over the orientation angle θ . Note the lack of indirect paths after 10 ns delay.

D. Results of the Outdoor Experiment

To qualify the results of the indoor experiment, another experiment was conducted outdoors. Fig. 6 shows the processed channel responses in the outdoor environment preventing as much indirect paths as possible. The same rotations as in the indoor experiment are performed outdoors. The rotation around the X axis shows a strong direct path and a weaker second path. The direct path has minor dents at 0° and 180° . Similar to the indoor experiment, the rotation around the Y axis shows a more scattered behavior of the channel response compared to the X axis. A similar pattern is observable assessing the rotation around the Z axis. A strong indirect path is visible at 6 ns, corresponding with the distance of the indirect path through ground reflections. As with the indoor experiment, strong dents are observable at 90° and 270° .

E. Deep Learning on Channel Response Data

In order to qualitatively assess the channel response data for machine learning approaches, the datasets of each experiment are analyzed using the RapidMiner [10]. The Deep Learning algorithm uses the implementation of H2O 3.8.2.6 [11]. As depicted in Fig. 7 a dataset is analyzed using a split data approach. A subset of the data is used to train a multi-layer feed-forward artificial neural network with 3 hidden layers, 50 neurons each. The split ratio of 80/20 was chosen using 80% for training and 20% for testing. In a next step the trained model is used on the remaining untrained data to estimate the ranging error corresponding with the channel response.

The results of the error estimation are depicted in Fig. 8. The true error and the predicted error using the deep learning algorithm are shown in the upper part of the figure. The line of equilibrium, where true and predicted error are equal is depicted for reference. In all three experiments the true and predicted error show good correspondence. To qualitatively assess the results, the cumulative distribution function $\Phi(\chi)$ of the ranging error χ is shown in the lower part of Fig. 8. It is clearly visible, that error prediction using a deep learning network improves the ranging significantly in this specific setup. However, a more general approach has to be considered using a larger dataset covering significantly more positions and orientations in future work. The raw channel response data will only be useful in conjunction with other sensor data such as inertial measurement unit data or leading edge detection diagnostic data as proposed in [7].

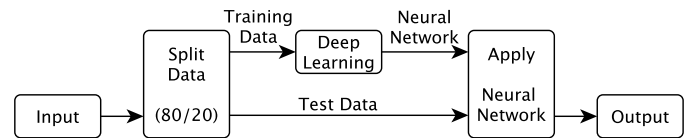


Fig. 7. Schematic illustration of the data flow used for the deep learning evaluation. The data is split with 80% of the data used for training and 20% for testing.

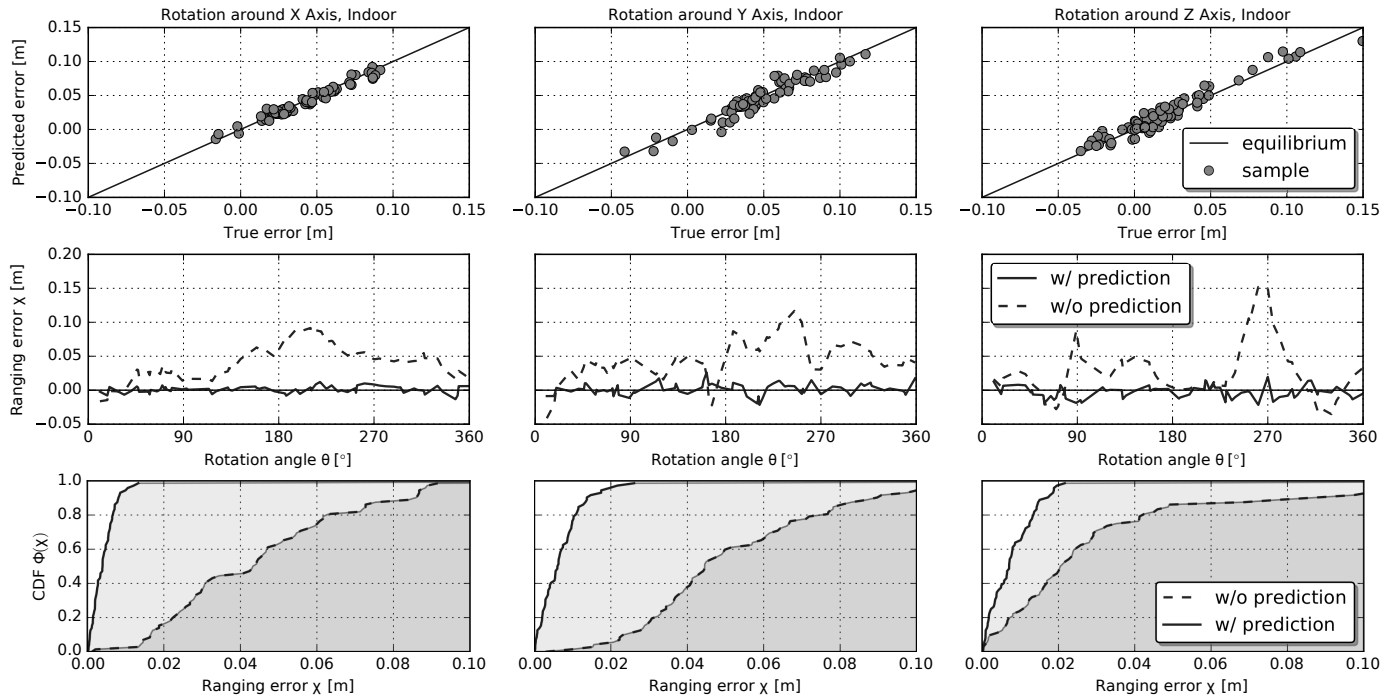


Fig. 8. Results of the proposed model application on the trained deep learning network. The predicted and the true ranging error χ are depicted in the upper section. The middle section demonstrates the ranging error with and without prediction over the rotation angle. The lower section depicts the cumulative distribution function (CDF) of ranging error without prediction and the remaining error when applying prediction on the measured ranges.

IV. CONCLUSION AND FUTURE WORK

This paper evaluates the orientation dependent characteristics of modern, integrated ultra-wideband transceiver experimentally. A suggestion for the optimal mode of operation in terms of orientation is derived from the presented results. The first path ratio classification is implemented and evaluated. The results show, that for accurate error prediction, more advanced methods are necessary. A novel method using deep learning on channel response data to improve ranging accuracy is proposed and evaluated experimentally. In a first static environment promising results show the potential for future applications as the accuracy is improved significantly through error prediction.

However, future work has to prove the general applicability of deep learning approaches on channel response data for dynamic environments. It is very likely that, depending on the application scenario, multi-parameter systems using inertial measurement unit data and more receiver diagnostics are necessary to achieve reliable results. In a next step, it is planned to integrate those approaches in a real-time positioning system to evaluate the accuracy depending on the chosen training data in dynamic indoor scenarios. The raw experimental datasets are provided alongside this work [9].

ACKNOWLEDGEMENT

The work on this paper has been partially funded by Deutsche Forschungsgemeinschaft (DFG) within the Collaborative Research Center SFB 876 “Providing Information by Resource-Constrained Analysis”, project A4 and was supported by the federal state of Northrhine-Westphalia and the “European Regional Development Fund” (EFRE) 2014-2020 in the course of the “CPS.HUBNRW” project under grant number EFRE-0400008.

REFERENCES

- [1] IEEE Std 802.15.4-2011: Part 15.4: Low-Rate Wireless Personal Area Networks (LR-WPANs). <http://standards.ieee.org/getieee802/download/802.15.4-2011.pdf>.
- [2] J. Tiemann, F. Schweikowski, and C. Wietfeld. Design of an UWB indoor-positioning system for UAV navigation in GNSS-denied environments. In *Indoor Positioning and Indoor Navigation (IPIN), 2015 International Conference on*, Oct 2015.
- [3] J. Tiemann, J. Pillmann, S. Boecker, and C. Wietfeld. Ultra-wideband aided precision parking for wireless power transfer to electric vehicles in real life scenarios. In *IEEE Vehicular Technology Conference (VTC-Fall)*, Montreal, Canada, Sep 2016.
- [4] M. Sharma, C. G. Parini, and A. Alomainy. Influence of antenna alignment and line-of-sight obstruction on the accuracy of range estimates between a pair of miniature UWB antennas. In *9th European Conference on Antennas and Propagation (EuCAP)*, May 2015.
- [5] J. Blumenstein, A. Prokes, A. Chandra, T. Mikulasek, R. Marsalek, T. Zemen, and C. Mecklenbraeuer. In-vehicle channel measurement, characterization and spatial consistency comparison of 3-11 GHz and 55-65 GHz frequency bands. *IEEE Transactions on Vehicular Technology*, PP(99):1–1, 2016.
- [6] DecaWave Ltd. *DW1000 User Manual - How to use, configure and program the DW1000 UWB transceiver 2.02*, 2014.
- [7] F. Hartmann, C. Enders, and W. Stork. Ranging errors in UWB networks and their detectability. In *2016 39th International Conference on Telecommunications and Signal Processing (TSP)*, June 2016.
- [8] Klaus Witrisal, Paul Meissner, Erik Leitinger, Yuan Shen, Carl Gustafson, Fredrik Tufvesson, Katsuyuki Haneda, Davide Dardari, Andreas F Molisch, Andrea Conti, et al. High-accuracy localization for assisted living: 5G systems will turn multipath channels from foe to friend. *IEEE Signal Processing Magazine*, 33(2):59–70, 2016.
- [9] J. Tiemann. Raw datasets of the rotation experiments, <http://dx.doi.org/10.5281/zenodo.228127>. Jan 2017.
- [10] Markus Hofmann and Ralf Klinkenberg. *RapidMiner: Data Mining Use Cases and Business Analytics Applications*. Chapman & Hall, 2013.
- [11] Arno Candell, Erin LeDell, Viraj Parmar, and Anisha Arora. *Deep Learning with H2O*. 2015.